Summary of Studies of the Response of a Prototype SiD ECal

Amanda Steinhebel, James Brau
University of Oregon, Center for High Energy Physics,
1274 University of Oregon Eugene, Oregon 97403-1274 USA
(Dated: March 5, 2018)

SiD is one validated detector design for the International Linear Collider (ILC) with strengths in particle flow calorimetery. The silicon — tungsten electromagnetic calorimeter (ECal) greatly contributes to this. Layers of highly granular (13 mm^2 pixels) silicon detectors embedded in thin gaps ($\sim$ 1 mm) between tungsten alloy plates give the SiD ECal the ability to separate electromagnetic showers in a crowded environment. A nine-layer prototype (5.8 X_0) was built and tested in a 12.1 GeV electron beam at SLAC National Accelerator Laboratory. This data was simulated with a Geant4 model. Particular attention was given to the separation of nearby incident electrons, which demonstrated a high (98.5%) separation efficiency for two electrons at least 1 cm from each other. In the future, this beam test study will be compared to a full SiD detector simulation.

I. KPIX BACKGROUND

SiD is one of two validated detector designs being considered for the International Linear Collider (ILC) [1]. Its electromagnetic calorimeter (ECal) is a solid-state sampling calorimeter constructed with alternating layers of silicon sensors and DENS-24, a tungsten alloy used as an absorber. The silicon layers are pixelated, and each pixel is individually read out by a KPiX ASIC chip [2]. This readout method is under consideration both for the tracker and ECal of SiD. The calorimeter's design and sensitivity are important elements of SiD's particle flow technique.

Thirty-one 0.3 mm thick silicon layers are created from tiled hexagonal wafers each containing 1024 individual 13 mm^2 pixels. As a photon or electron from the collision passes through the ECal, the tungsten layers induce showering. The silicon layers then measure any charge deposited on them as the shower progresses through the calorimeter. One KPiX readout chip is bump-bonded to the center of each silicon wafer (Fig. 1) that is connected via channels to each pixel on the chip. The use of KPiX allows for thin gaps between absorber layers of 1.25 mm (Fig. 2), where the silicon sensors, KPiX chip, and electronics sit.

Prototype versions of silicon wafers mounted with KPiX chips and cables were tested at SLAC National Accelerator

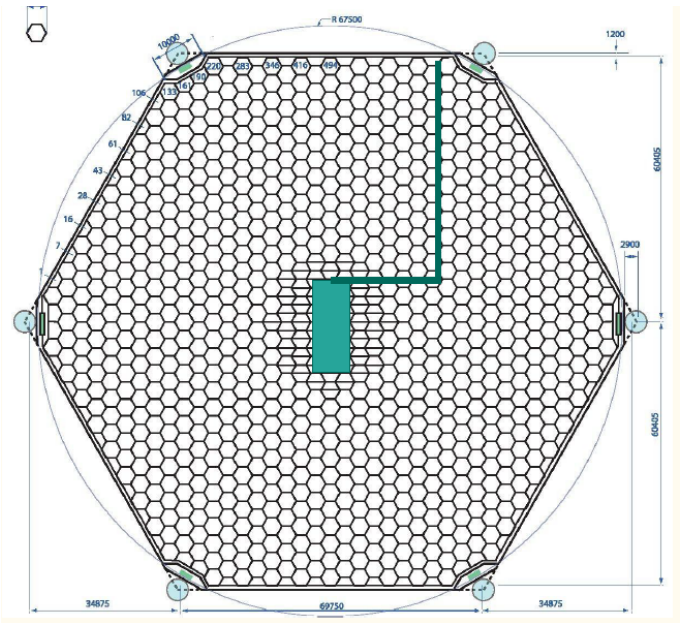

FIG. 1: The engineering schematic of one ECal silicon wafer, with the position of the KPiX readout chip shown in green in the center of the wafer [1].

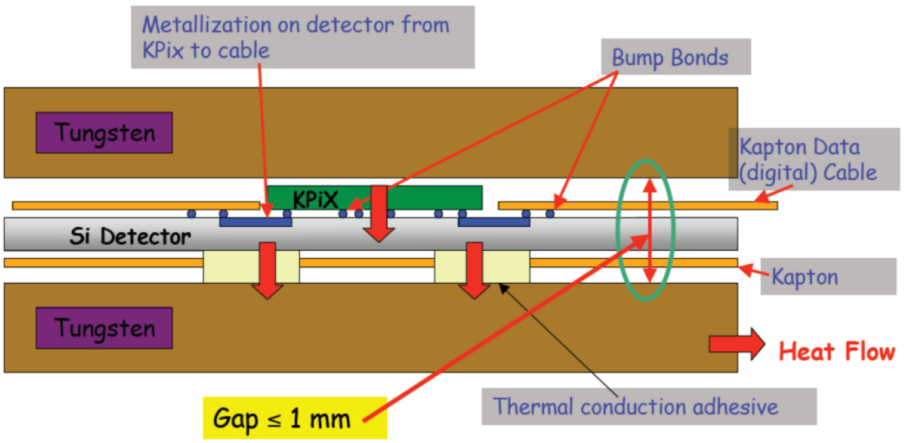

FIG. 2: The 1.25 mm gap between tungsten absorber layers includes a 0.3 mm silicon sensor layer bump-bonded to the KPiX readout chip. [Figure credit: Martin Breidenbach, SLAC]

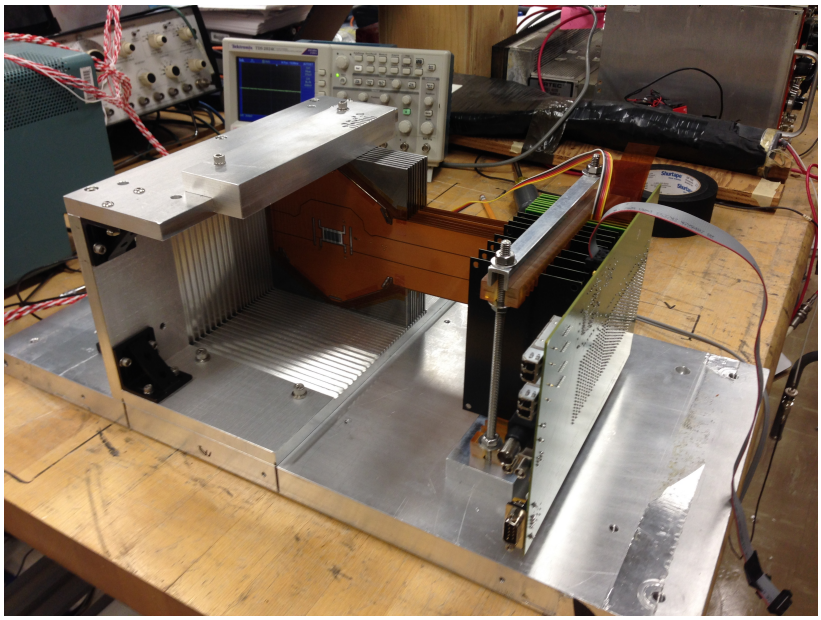

FIG. 3: The ECal prototype setup at SLAC, in a silicon-first arrangement. [Photo credit: Marco Oriunno, SLAC]

Laboratory in 2013 to measure the response of the calorimeter [3]. The prototype calorimeter consisted of nine paired layers of silicon wafers and 2.5 mm DENS-24 plates (Fig. 3), for a total expanse of 5.8 X_0. A 12.1 GeV electron beam was directed through the prototype calorimeter, and the KPiX response was recorded. The alternating silicon/tungsten pattern allowed for testing with both silicon- and tungsten-first setups.[1]

[1] For silicon-first runs, silicon layers are labeled 8 → 0 with Layer 8 being the upstream layer. Tungsten-first runs are reversed, with Layer 0 as the upstream layer.

Table I indicates the data runs used in this study, as well as any comments on the run from the SLAC Day Log. All runs were conducted with an EVR trigger rate of 5 Hz, one intended particle per pulse, and a DacThresholdA of 240 with a null DacRangeThreshold.[2]

All figures shown here can be found at `http://pages.uoregon.edu/asteinhe/SiDNotes/testBeamStudies`. The analysis scripts used to generate them can be found as well, at `https://github.com/SiliconDetector/UserAnalyses/tree/master/asteinhebel_ECalAnalysis/testBeamStudies`.

TABLE I: Data files used for analysis of KPiX performance in the 2013 SLAC prototype studies.

File	Layer Ordering	Comments on Data Quality	Shorthand Label
2013_07_26_10_41_28	$8 \rightarrow 0$ (Si-first)	None	28
2013_07_26_14_13_43	$8 \rightarrow 0$ (Si-first)	Brief "dead beam" gap near end of run	43
2013_07_29_16_12_24	$0 \rightarrow 8$ (W-first)	Recorded whole layers activating	24

II. BEAM TEST MODELING STUDIES

A. Silicon-First Beam Test Analysis

Before the analysis, the beam test data was cleaned. This cleaning included the removal of "monster events", or events in which all pixels inappropriately reported a large amount of deposited charge. This phenomenon has since been understood and corrected.

After the monster events were removed, a large number of low energy events remained from the data set of more

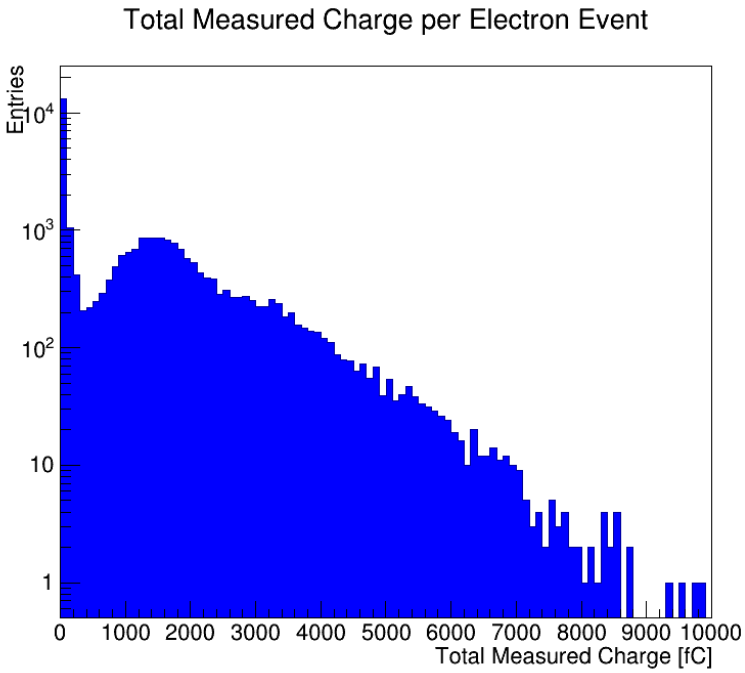

FIG. 4: Total measured charge per event from the beam test where the silicon layer was placed first. Note the large peak of low energy events, as well as clear peaks around intervals of roughly 1500 fC indicating electron events.

[2] DacThresholdA sets the threshold for individual pixels to internally trigger on events. DacRangeThreshold causes the detector to switch to a low-gain mode if the total signal is above a certain threshold. The default value of zero, used here, prevents the chip from ever switching into this low-gain mode.

than 30,000 events (Fig. 4)[3]. These were accompanied by peaks at intervals of roughly 1500 fC, indicating electron events. The peaks at higher measured charge are multiple electron events.

Many low energy events are soft photon contamination from the electron beam, or under-developed electron showers that begin to shower late into the calorimeter resulting in high leakage unmeasured by the short 5.8 X_0 prototype. Setting a higher threshold on the recorded charge would eliminate the consideration of this contamination, but also neglect low shower-energy electron events. In order to clean out only the contamination without implimenting a simple cut that would eliminate low-energy electron showers, an algorithm was designed to categorize showers. In this way, "photons" could be separated from "electron" showers and eliminated.

One simple categorization technique counts how many layers of silicon record measured charge in a given event. Roughly 45% of events only deposit charge in one layer (Fig. 5). Of those events, nearly 71% deposited charge late in the detector in Layer 2, 1, or 0 (Fig. 6) and may be due to late-developing showers that could not be adequately contained within the prototype. Events with only one layer containing measured charge are considered to be contamination, and were removed from consideration.

A weighting algorithm was developed to further categorize showers. The silicon layers were re-labeled from $1 \rightarrow 9$, with Layer 1 the upstream layer for discrimination purposes only. Then, the ratio

$$R = \frac{\sum_h L_h^2 \mathcal{C}_h}{\sum_h \mathcal{C}_h} \tag{1}$$

was calculated using the re-labeled layers, where $\mathcal{C}_h$ is the measured charge for a given hit and L_h is the layer number of the hit, summed over all hits h. If for some layer there were no hits, a deposit of 4 fC was inserted. This is roughly the charge that a minimum ionizing particle would deposit.

Soft photon events or under-developed showers tend to only deposit charge in a few layers of the detector, causing R to be small. Alternately, electron showers traverse through more of the detector and increase R (Fig. 7). A cut on R was applied where $R = 44$, and events with R less than the cut value were disregarded as soft photon contamination or undeveloped showers.

After this procedure, nearly 50% of all events from the data set were removed. The resulting data set (Fig. 8) retains low shower-energy electron events while the large photon contamination peak has been removed.

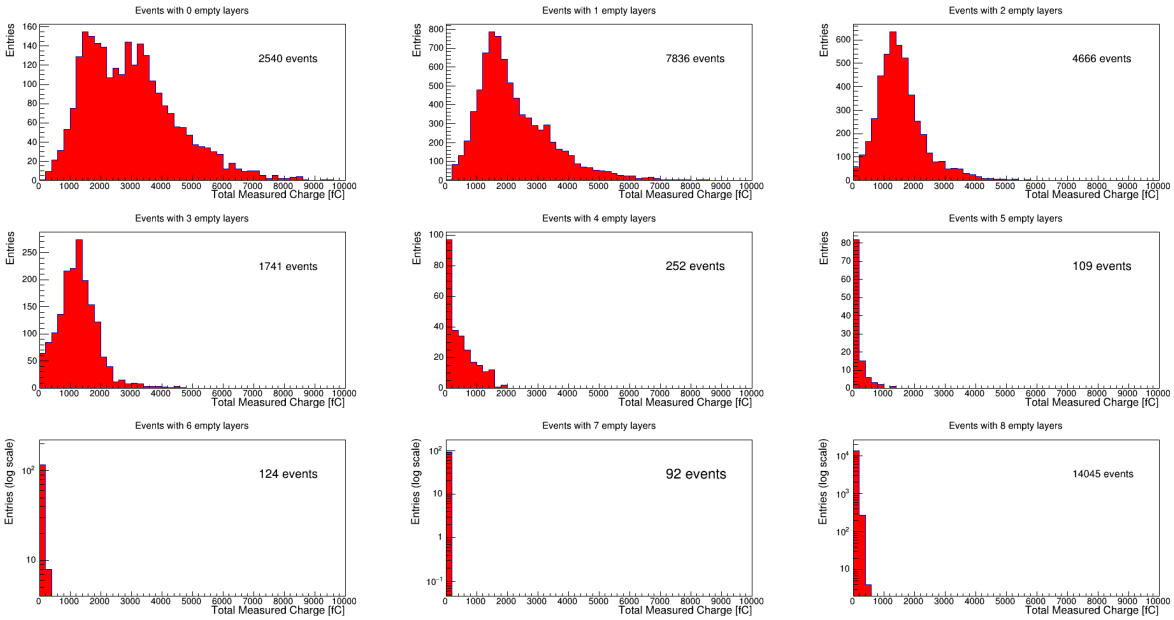

FIG. 5: The number of events with recorded charge deposits in a certain number of layers. Roughly 45% of events only deposit charge in one layer of the detector (see Fig. 6).

[3] Unless otherwise stated, data shown corresponds to silicon-first Run 43. Analogous plots for Run 28 can be found in Section VIII A. Special attention is paid to tungsten-first Run 24 in Section III.

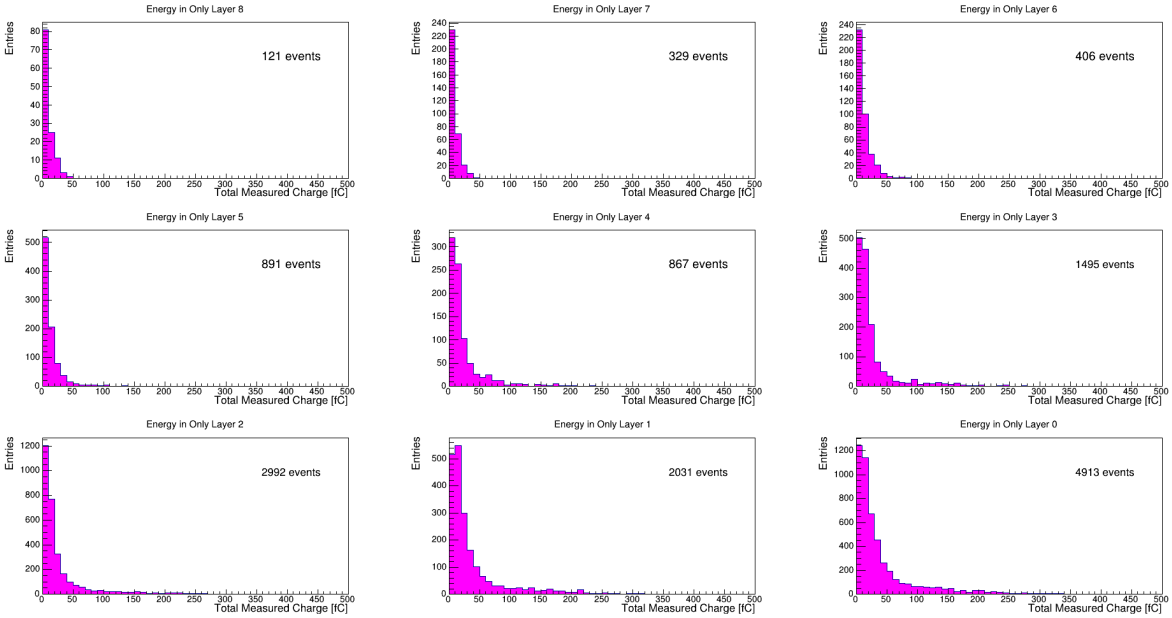

FIG. 6: For events that only deposit charge in one single layer of the detector, the layer of detected charge deposition is shown. Nearly 71% of these events deposit deep into the calorimeter (in Layer 2, 1, or 0). Figures are shown in upstream order (where the beam encounters Layer 8 first and Layer 0 last).

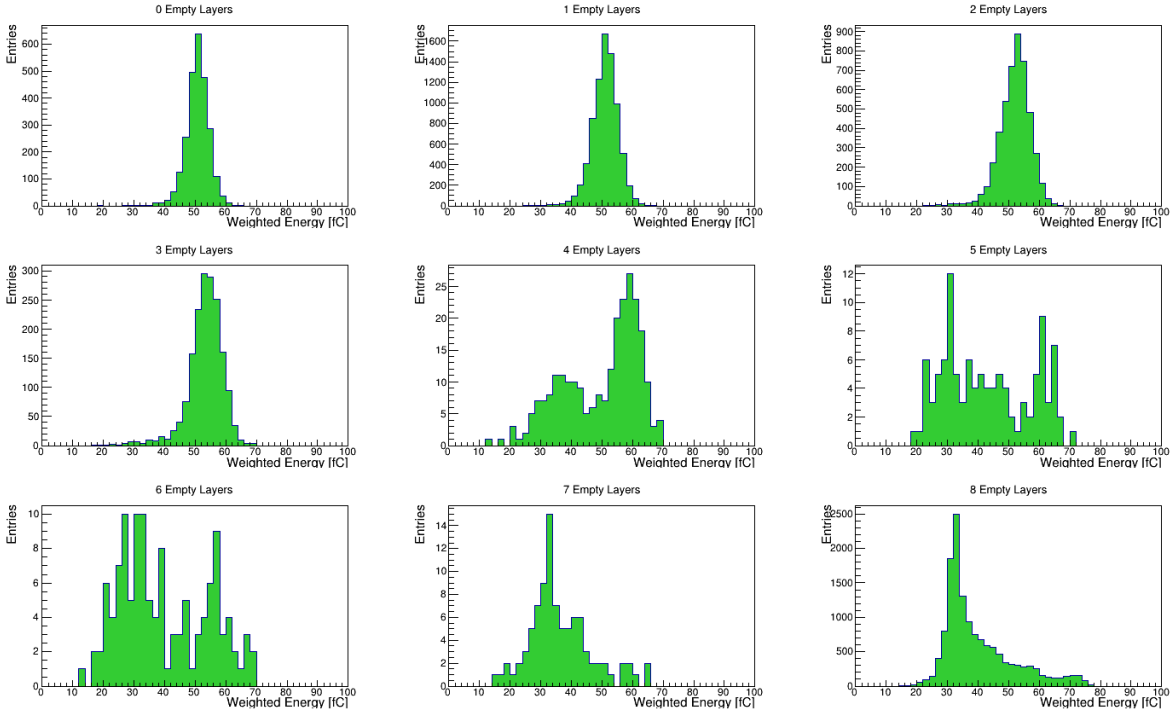

FIG. 7: Value of the statistic of Eqn. 1, separated by how many empty layers were in the event. Events with few empty layers had larger values of R, while events with many empty layers had low R values and were categorized as contamination when $R < 44$. The "8 Empty Layers" figure (bottom right) illustrates a distribution containing nearly all contaminants. All events with eight empty layers are removed as contamination regardless of their R value.

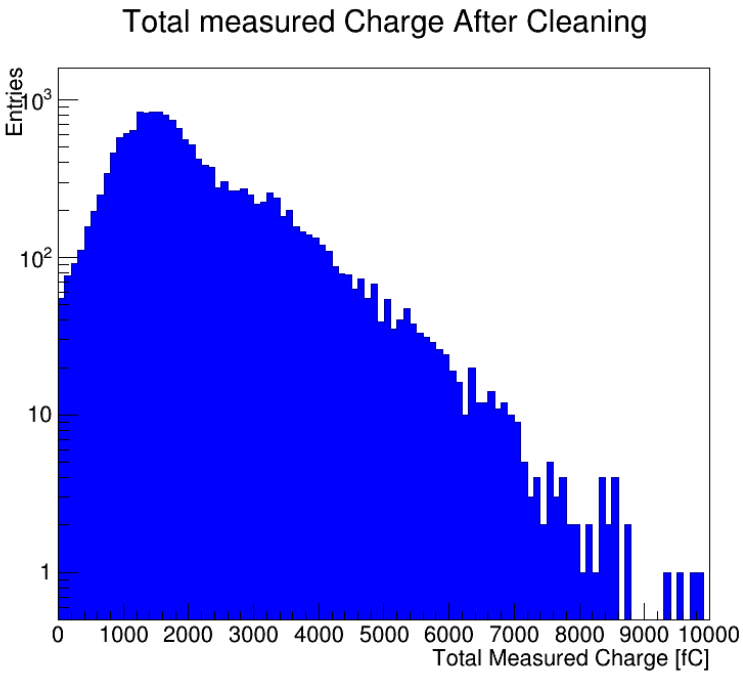

FIG. 8: Deposited charge data from the beam test where the silicon layer was placed first, after removing contamination.

B. Silicon-First Simulation Analysis

A Geant4 simulation was created to model the beam test scenario. The simulation consisted of 8,000 single electron events transversely distributed in the calorimeter to match the beam test data (Fig. 9). The measured energy distribution of these events is easily fit with a Gaussian (Fig. 10).

The collection of single-electron events was then used to create a Poisson distribution of multi-electron events up to five electrons by overlaying multiple single-electron events. Using a fitting algorithm based upon the beam test data, a Poisson mean of $\langle n \rangle = 0.8725$ was used to replicate the beam test results (see Section VIII B). In order to simulate inactive pixels observed during the beam test, 10% of the pixels of each layer were randomly removed. The tungsten alloy DENS-24 was modeled by including a layers of pure tungsten and nickel in the simulation. This approximately matched both the thickness and dE/dx of the alloy. The resulting data set is shown in Fig. 11.

The simulated and collected data agree well (Fig. 12), after normalization and the application of a conversion factor of 29.575 MeV $\cong$ 1 fC (found by fitting the beam test data as detailed in Sec. VIII B). This agreement holds not only for the total measured charge in each event, but for the total measured charge in each layer of the prototype detector as well (Fig. 13).

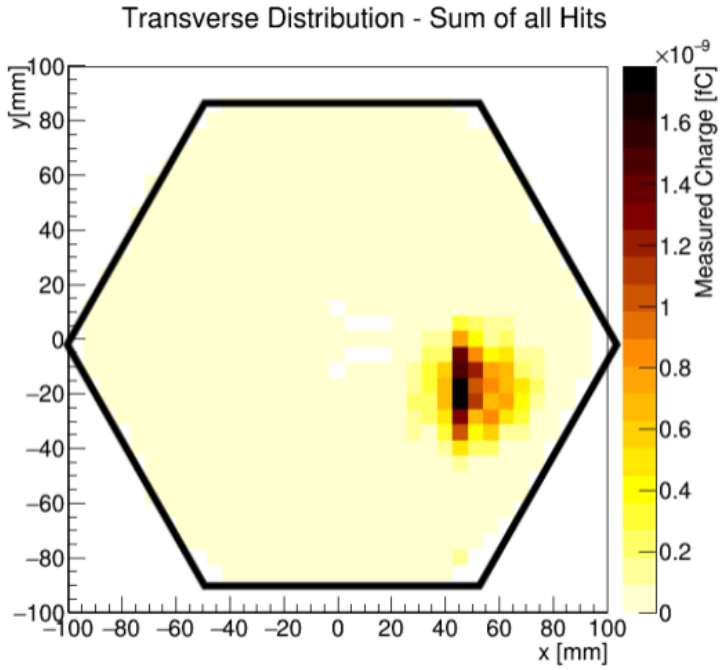

FIG. 9: Profile of the position of hits in the ECal prototype. The intensity of color indicates the amount of measured charged summed over all nine layers at that xy position, with a solid line indicating the edge of the wafer. Incident electrons simulated with Geant4 mimic this distribution.

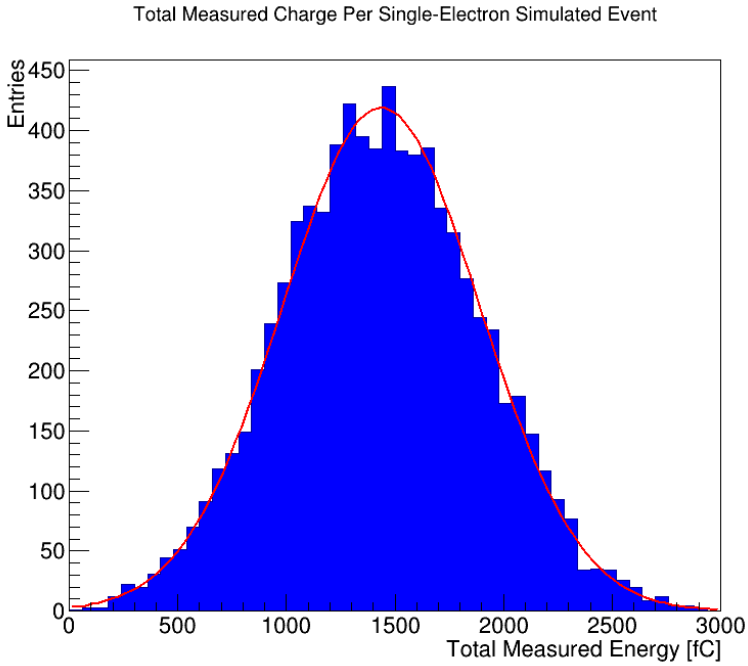

FIG. 10: Total measured energy in Geant4 simulated single electron events fit with a Gaussian.

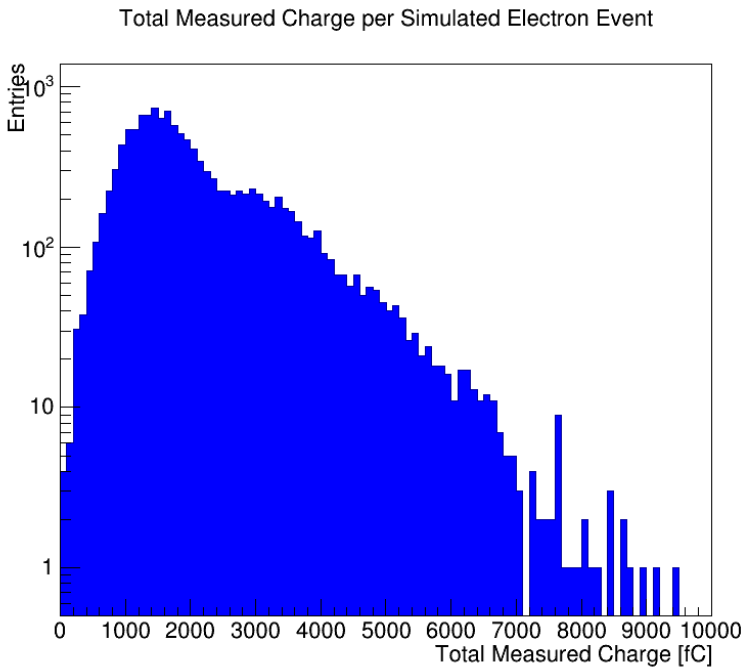

FIG. 11: Geant4 simulated data designed to match the beam test prototype.

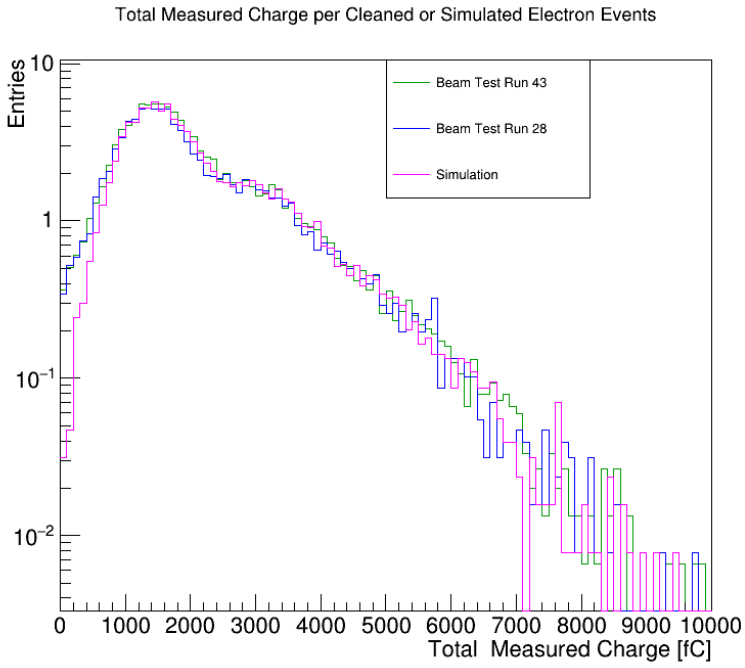

FIG. 12: Two silicon-first prototype runs match very well with Geant4 simulated data when the total measured charge in each event is compared after the prototype data sets are cleaned of contamination.

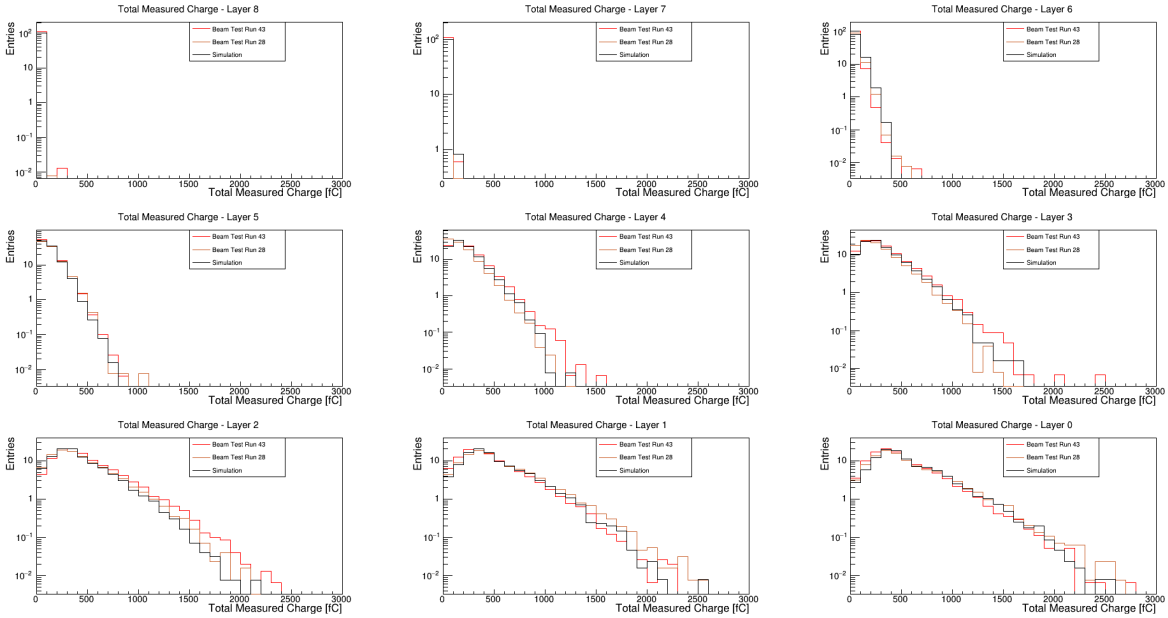

FIG. 13: Two silicon-first prototype runs match very well with Geant4 simulated data when the total measured charge in each layer of each event is compared after the prototype data sets are cleaned of contamination.

III. TUNGSTEN-FIRST RUNS

Tungsten-first runs were conducted at the end of the SLAC data taking period. A similar contamination problem was noted in Run 24 (see Table I) and corrected for in an identical manner as the silicon-first runs as explained in Section II (Fig. 14).

Due to the quicker shower evolution due to the first layer being tungsten, a cut on the statistic of Eqn. 1 was made at $R = 40$ (Fig. 15). For tungsten-first runs, layer labeling for the statistic simply consisted of adding one (1) to each layer number, thus no layer reversing was done (as in the silicon-first case). After an identical veto requiring both that events contain deposits in more than one layer and an R value greater than 40, the data was cleaned of contamination while retaining low shower energy electrons (Fig. 16).

The simulation was optimized in an identical manner for the tungsten-first runs, using a tungsten-first setup in simulation as well. In this orientation, single-electron events are still appropriately fit with a Gaussian (Fig. 17). In this case, the Poisson mean was $\langle n \rangle = 0.773$ with conversion factor 29.39 MeV $\cong$ 1 fC. These values differ from the silicon-first ones due to independent fitting procedures (see Sec. VIII B). The simulated distribution can be seen in Fig. 18. Again, the cleaned beam test data and simulation data set agreed, though less well than those of the silicon-first runs (Figs. 19 and 20).

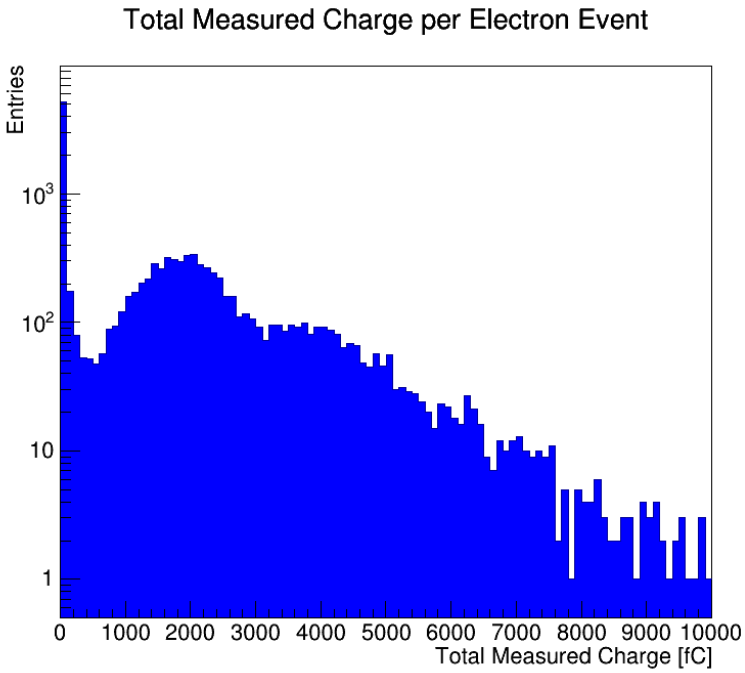

FIG. 14: Total measured charge per event from the beam test where the tungsten layer was placed first.

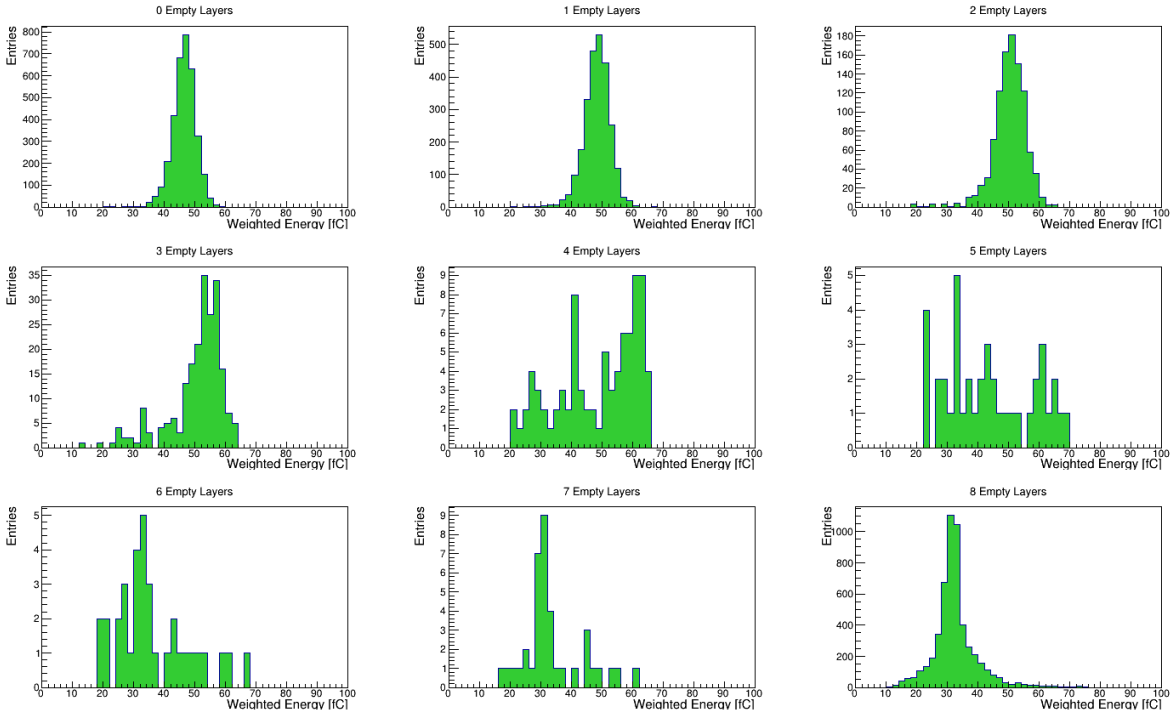

FIG. 15: Value of the statistic of Eqn. 1, separated by how many empty layers were in the event. Events with few empty layers had larger values of R, while events with many empty layers had low R values and were categorized as contamination when $R < 40$.

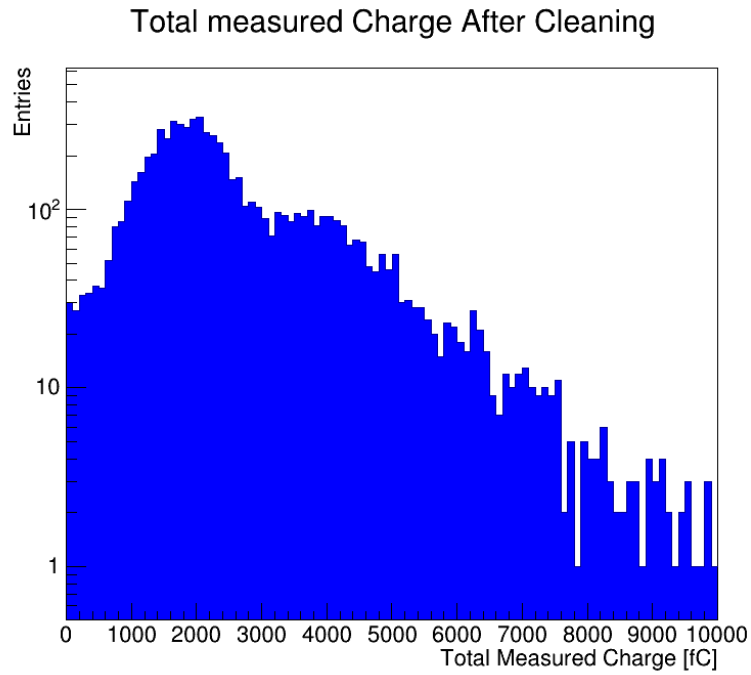

FIG. 16: Deposited charge data from the beam test where the tungsten layer was placed first, after removing contamination.

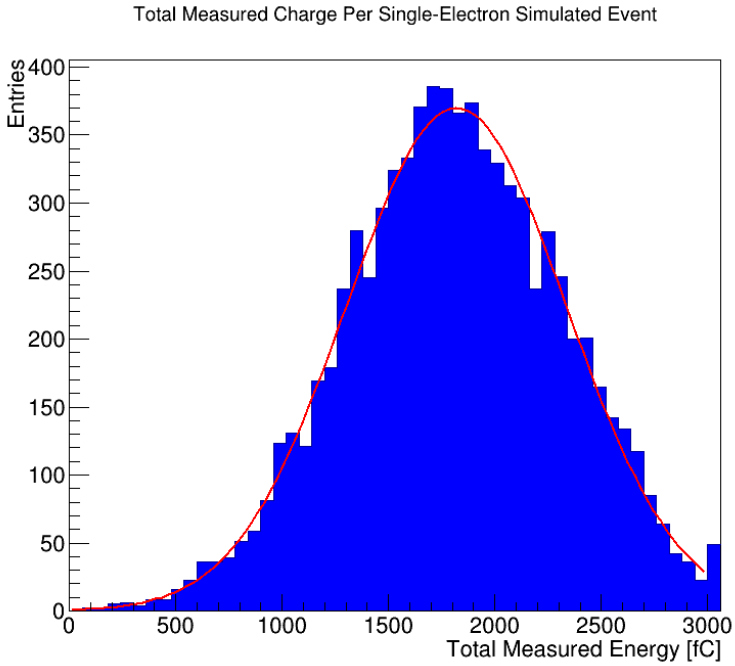

FIG. 17: Geant4 simulated single electron events fit with a Gaussian.

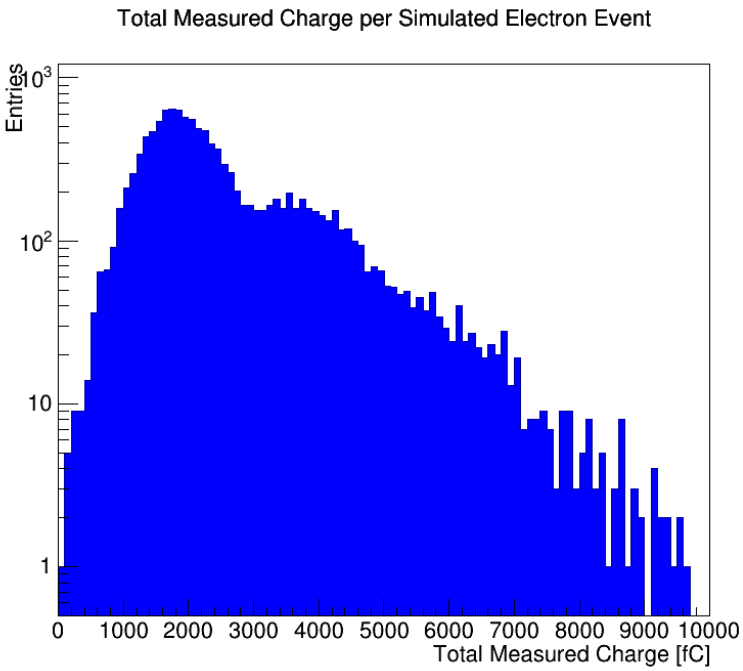

FIG. 18: Geant4 simulated data designed to match the beam test prototype.

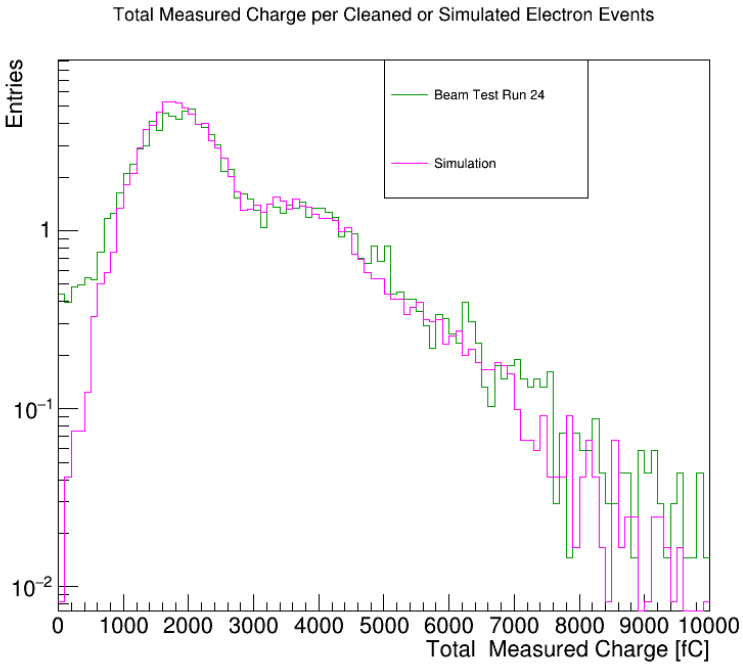

FIG. 19: The tungsten-first prototype matches with Geant4 simulated data when the total measured charge in each event is compared after the prototype data sets are cleaned of contamination.

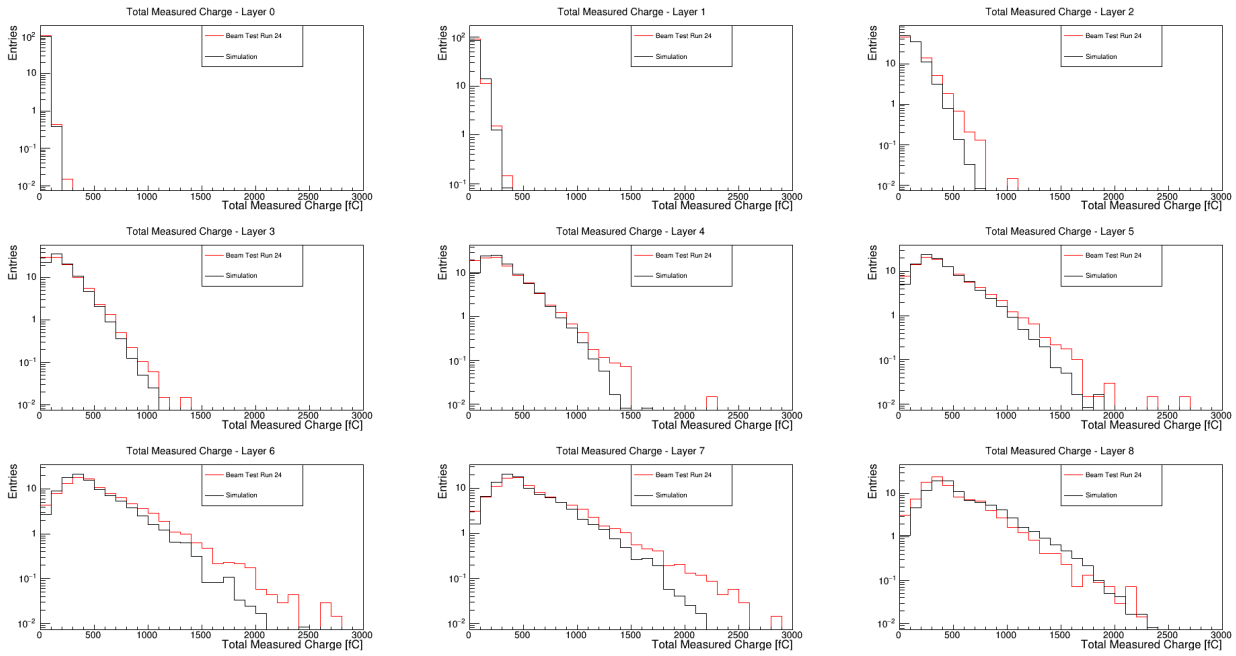

FIG. 20: The tungsten-first prototype matches with Geant4 simulated data when the total measured charge in each layer of each event is compared after the prototype data sets are cleaned of contamination.

The most significant source of disagreement in Fig. 20 is in the shape of the distributions of Layers 2, 6, and 7. This may be due to faulty wiring, or an inconsistency in the tungsten thickness paired with these silicon wafers. It also appears that beam test data Layers 7 and 8 should be swapped, perhaps resulting from mis-wiring. This run (see Table I) was also conducted near the end of data collection, and electronic issues were noted at the time of the run. Any of these aspects may have played into the noted difference between simulated and beam test data sets.

Another source of disagreement could be due to fluctuations in the data set not properly modeled by the simulation. An additional parameter was included in the fit to find the Poisson mean (see Sec.VIII B) that encompassed these extra fluctuations by finding an appropriate augmentation of the standard deviation of the Gaussian distribution that described simulated single-electron events. This takes additional experimental fluctuations into account in the simulation distribution. Silicon-first were found to require no such addition, but the correction was nonzero in the tungsten-first scenario. This additional experimental uncertainty was applied to hits in the simulation by adding an equal fluctuation to every hit in each event. After this fluctuation inclusion, the simulation and experimental data sets agree better than in Figs. 19 and 20, though still not as well as the silicon-first runs of Figs. 12 and 13 (Figs. 21 and 22). This discrepancy is thought to be attributed to the less well understood relative running conditions of the tungsten-first data sets.

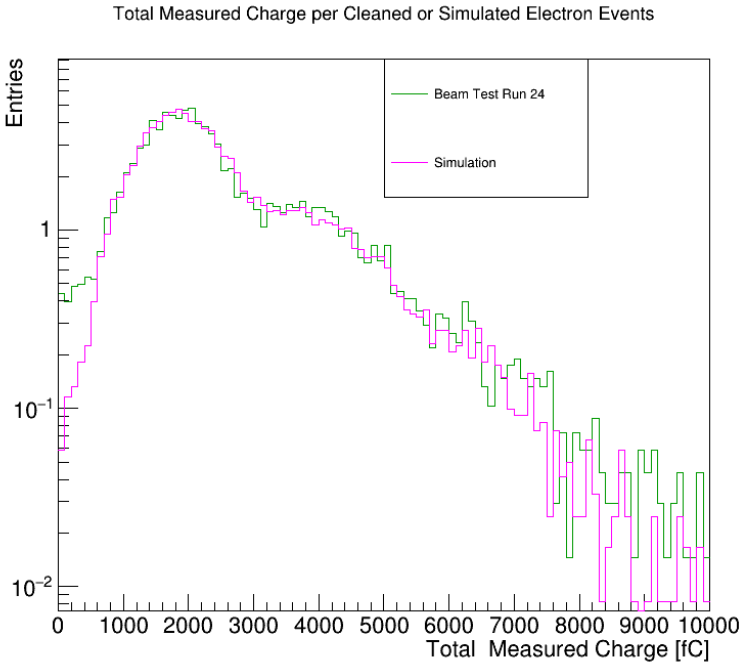

FIG. 21: The tungsten-first prototype matches better with Geant4 simulated data after additional statistical experimental fluctuations are included in the simulated data set.

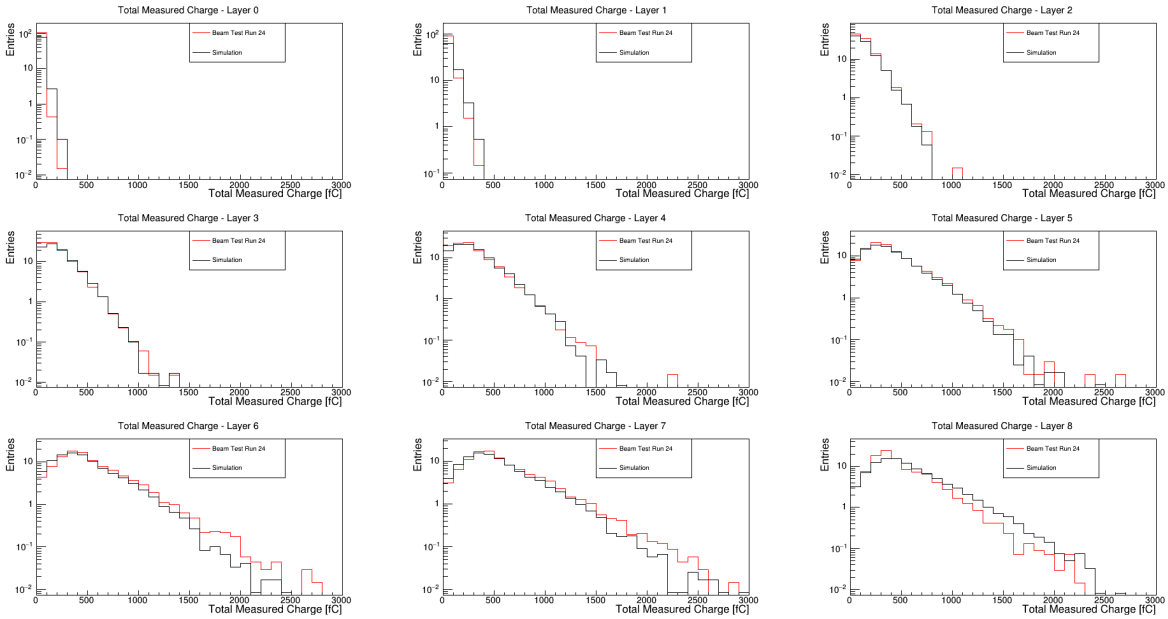

FIG. 22: The tungsten-first prototype matches matches better with Geant4 simulated data after additional statistical experimental fluctuations are included in the simulated data set, on an individual layer basis.

IV. ORIENTATION COMPARISON

For completeness, the orientation of the ECal prototype was also compared using both simulated and experimental data. To make a direct comparison, the first eight layers of the tungsten-first runs were used and offset by one layer so that each compared silicon layer had an identical amount of tungsten before it.

Overlaying the contaminant-free silicon- and tungsten-first beam test runs from Figs. 8 and 16 results in Fig. 23. Similarly, the simulation runs of Figs. 11 and 18 can be compared as in Fig. 24.

The degree of agreement is an accomplishment, both in simulation optimization but also in experimental data taking and KPiX performance. This being said, there are still a few inconsistencies with the comparison of experimental and simulated data. For example, the largest deviation is always found in Layer 2 (or Layer 6 for the silicon-first runs of Section II) where the tail of the beam test data distribution is more pronounced than that of the simulated data. This could be due to mis-wiring of the layers or irregularity of a tungsten layer, as stated in Section III.

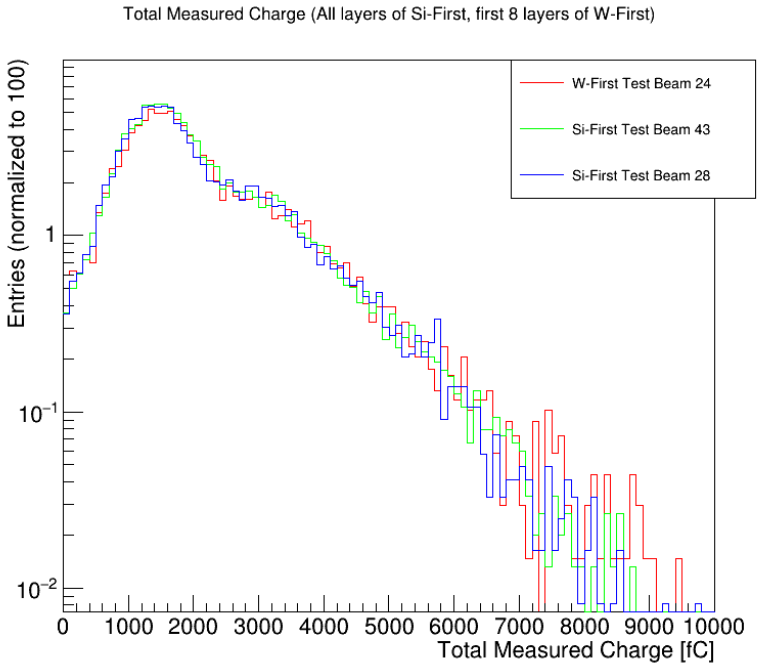

FIG. 23: The cleaned tungsten- and silicon-first beam test runs agree, regardless of orientation (when only the first eight layers of the tungsten-first run are considered).

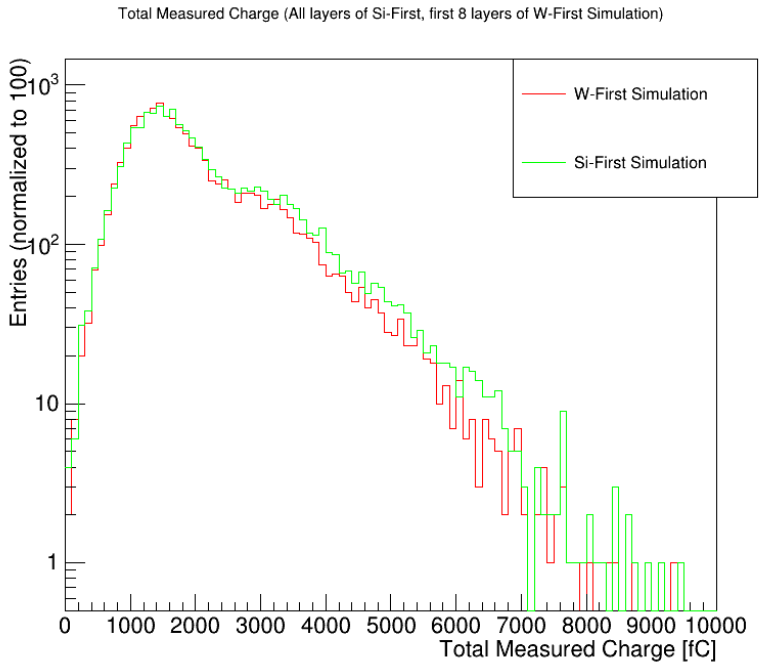

FIG. 24: The cleaned tungsten- and silicon-first simulation runs agree, regardless of orientation (when only the first eight layers of the tungsten-first run are considered).

V. SHOWER SEPARATION EFFICIENCY STUDIES

The high spatial granularity provided by the silicon pixels and KPiX can help distinguish the showers of two nearby particles. Since two-electron events were clearly observed in the beam test prototype run, a study of the prototype's ability to separate showers was performed. An algorithm was created to count the number of incident particles detected in each event. This algorithm is simple in nature, but robust enough to examine data from both the beam test prototype and Geant4 simulation. It requires inputs that describe the geometry of the silicon wafer, including which pixels border which other pixels, and the charge measured in each pixel. The algorithm examines each layer of each event and determines local maxima of charge deposits. It then compares the position of this maximum against all other layers, and requires that the same pixel location be a local maximum in at least four layers. If this condition is met, then an electron event is counted. In this way, the algorithm can account for multiple electrons occurring within one event but it also biases against late forming showers that do not develop fully enough to create four layers with notable maxima.

Occasionally, a shower maximum was shared between two pixels as the particle moved through the detector. In this case, the recorded local maximum was equally likely to be located in either pixel. This fooled the algorithm into tagging two incident particles though there was truly only one. The counting of more incident electrons than expected is considered "over-counting". The algorithm corrects for this by disallowing the presence of maxima in neighboring pixels.

With simulated data, information regarding the number of incident electrons is available and the accuracy of the algorithm can be examined. Figure 25 shows the algorithm's response to the full data set of all electron events. The algorithm counts correctly for more than 90% of events, and the majority of failures stem from under-counting.

Among simulated two-electron events, the algorithm correctly counted 82.6% of events (Fig. 27). 17.3% of two-electron simulated events were under-counted, reflecting a similar trend to the counting of the full data set (Fig. 26). When events were incorrectly under-counted, the two electrons tended to be less than 1 cm apart. This is due both to potential overlap of the close showers and also the pixel size themselves. From corner to corner, each pixel measures 4.5 mm. Therefore, two showers within this range would have maximum deposits in the same pixel. The algorithm counted two-electron events with an average efficiency of 98.5% when the incident electrons were separated by more than 1 cm.

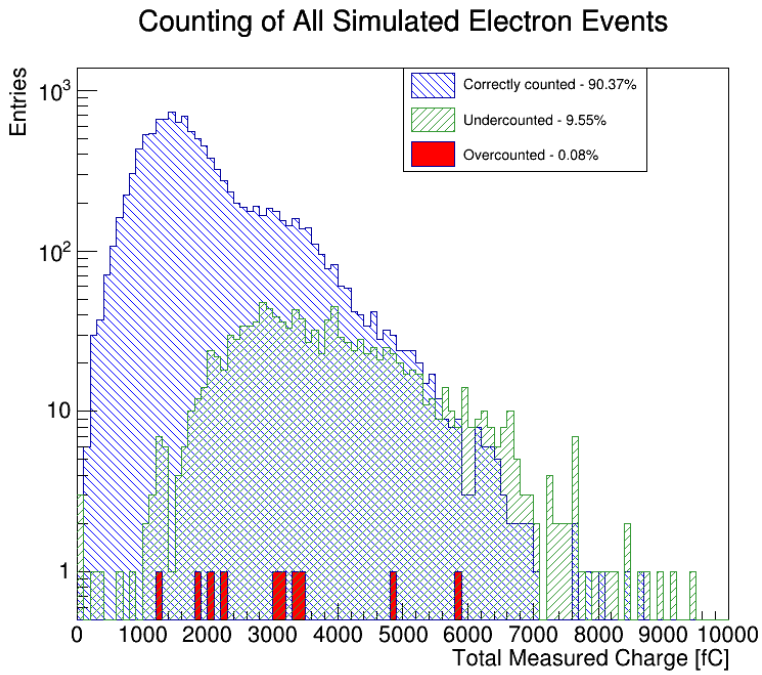

FIG. 25: Performance of the electron counting algorithm with all simulated events. The algorithm tends to correctly count electron events (right slant blue fill), but when miscounting under-counting (left slant green fill) is more common than over-counting (solid red fill).

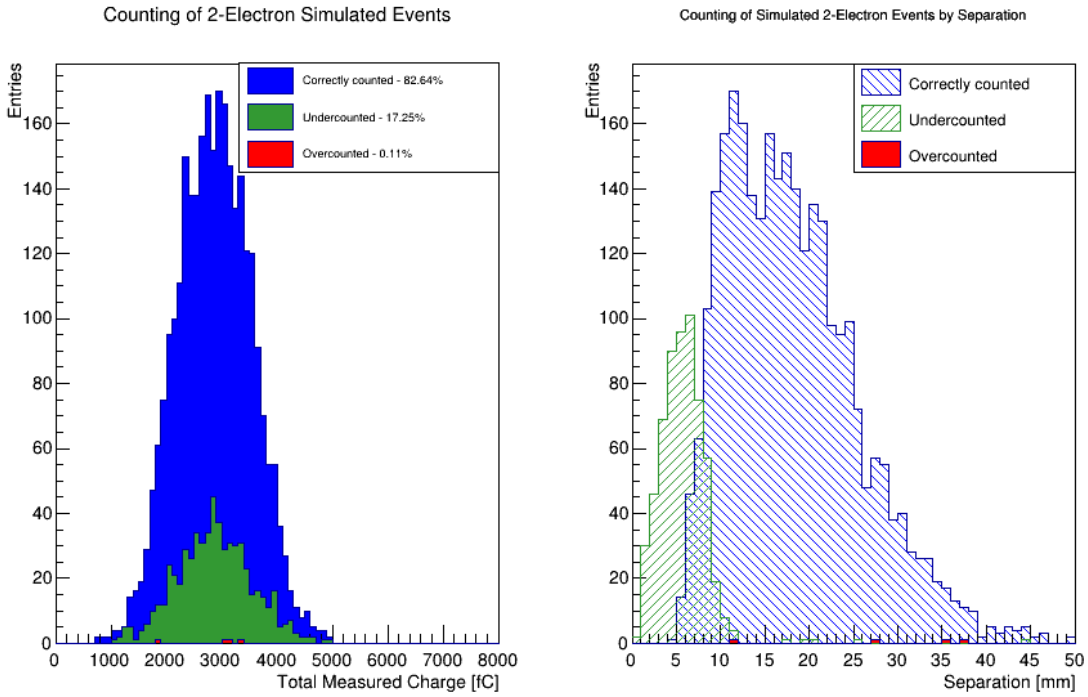

FIG. 26: Performance of the electron counting algorithm with simulated two-electron events. The algorithm tends to correctly count two electrons (right slant blue fill), but when miscounting under-counting (left slant green fill) is more common than over-counting (solid red fill). Under-counted events tend to occur when the two electrons were less than 1 cm apart.

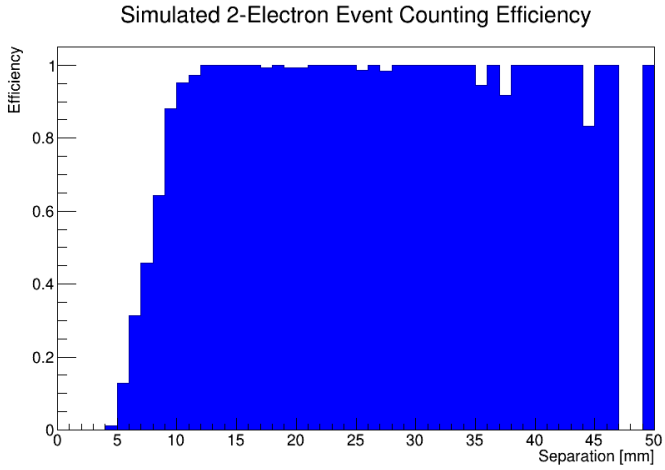

FIG. 27: Efficiency of electron counting algorithm with simulated two-electron events. When incident electrons were separated by more than 1 cm, the algorithm correctly counted two indicent particles with an average efficiency of 98.5%.

The algorithm can also analyze data from the beam test prototype. The results of the algorithm counting beam test events is shown in Fig. 28, and can be compared to the true simulation information (Fig. 29) and counted simulation events (Fig. 30). As before, the algorithm tends to under-count and in the beam test (Fig. 28) counts a significant number of "zero-electron" events (events where no electrons are counted).

Events the algorithm tags from the beam test data as "two-electron events" compare appropriately to those that the algorithm tags from the simulated data set. The algorithm performs well, as these distributions compare well to simulation information (Fig. 31). 4 mm bins here roughly indicate the size of one pixel. This indicates both that the simulation is correctly modeling the system, and that the algorithm can be trusted to identify multi-electron events in prototype data with nearly perfect efficiency provided that incident electrons are separated by more than 1 cm.

The ability to discern multiple electrons incident in close proximity is important for SiD's particle flow technique. Especially of interest is the ability to reconstruct boosted π^0 mesons from their decay products of two photons. This project is currently under investigation at the University of Oregon utilizing the SiD detector simulation and decays of Higgs bosons to two tau leptons.

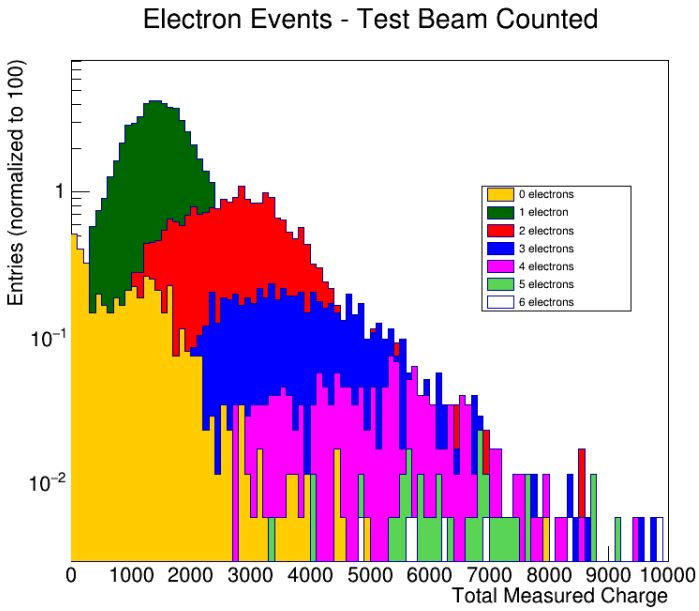

FIG. 28: Distributions of the number of counted electrons in silicon-first beam test Run 43.

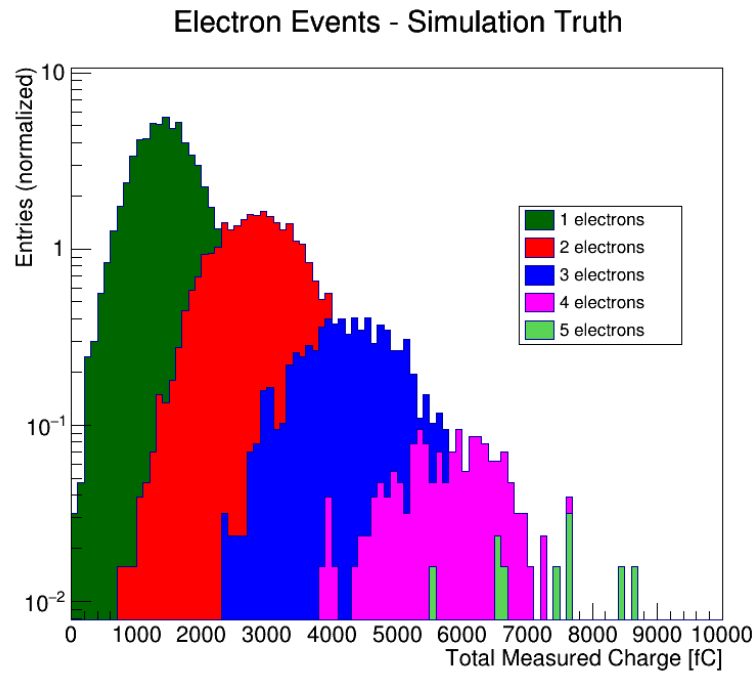

FIG. 29: Distributions of the number of true electron events in the silicon-first simulation.

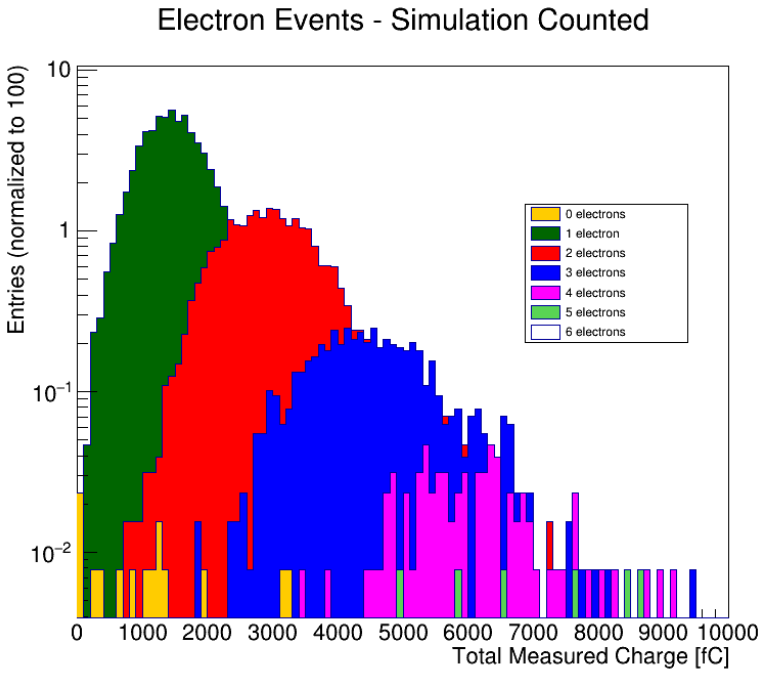

FIG. 30: Distributions of the number of counted electrons in the silicon-first simulation.

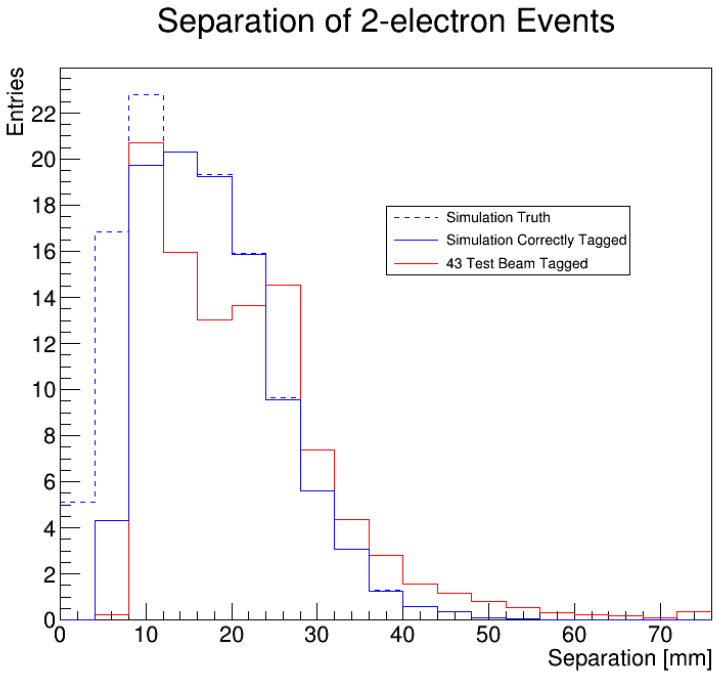

FIG. 31: The algorithm tags two-electron events from the beam test and simulated data at similar rates. The tagging is less accurate when the electrons are separated less than 1 cm. The two tagged distributions are normalized to 100 events for comparison. The tagged simulation distribution is a subset of the true simulation distribution (dotted).

VI. CONCLUSION AND FUTURE WORK

In preparation for the International Linear Collider, the SiD collaboration continues to work toward an optimized detector design and better understanding of the detector's performance and response. A crucial element of the detector is the solid-state silicon—tungsten sampling electromagnetic calorimeter. It is vital to SiD's particle flow technique, and its compact size makes it cost effective.

An early prototype of this ECal was constructed in 2013, complete with the KPiX ASIC readout chip, and its response to an electron beam was studied. A simulation was also designed to mimic the experimental environment. Both the experimental beam test and corresponding simulation have been studied and understood, as detailed above.

Using this information, an algorithm was created to count the number of incident electrons in each simulated and experimental event. This algorithm performs well, including in the case of two-electron events which are physically relevant due to their relation to boosted π^0 meson decays. If two showers are separated more than 1 cm in the beam test simulation, the algorithm can correctly count two events 98.5% of the time. Techniques used to achieve this can be applied to the full SiD detector simulation and used to analyze physics events.

VII. ACKNOWLEDGMENTS

We would like to thank Jason Barkeloo, Edouard Hay, Craig Gallagher, and Dylan Mead for their extensive previous work with the electron-counting algorithm and SLAC beam test data. We would also like to thank Jan Strube and the SiD Optimization group for their input and guidance.

VIII. AUXILIARY MATERIAL

A. Run 28

Two silicon-first runs from the SLAC prototype ECal were used for analysis (as detailed in Table I). Run 43 was largely used throughout the paper, though the trends are similar to the other silicon-first run, Run 28. Plots for Run 28, analogous to those shown in Sec. II A, are shown here.

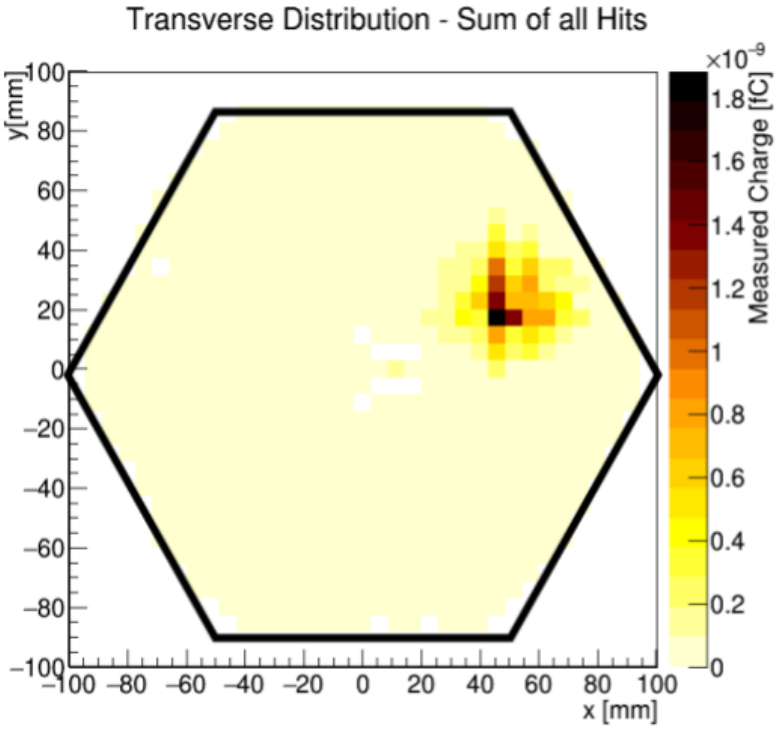

FIG. 32: Profile of the position of hits along the ECal prototype. The intensity of color indicates the amount of measured charged summed over all nine layers at that xy position, with a solid line indicating the edge of the wafer.

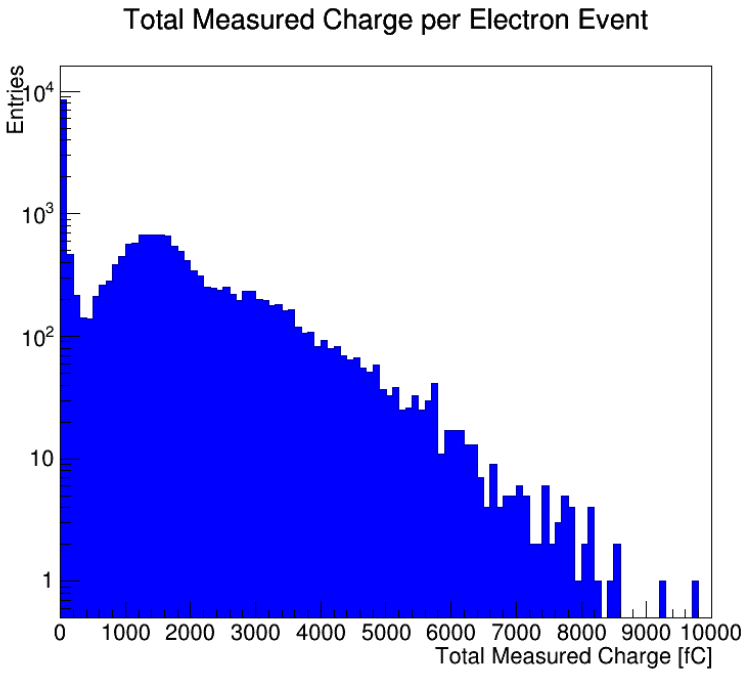

FIG. 33: Total measured charge per event from the beam test where the silicon layer was placed first. Note the large peak of low energy events, as well as clear peaks around intervals of 1500 fC indicating electron events.

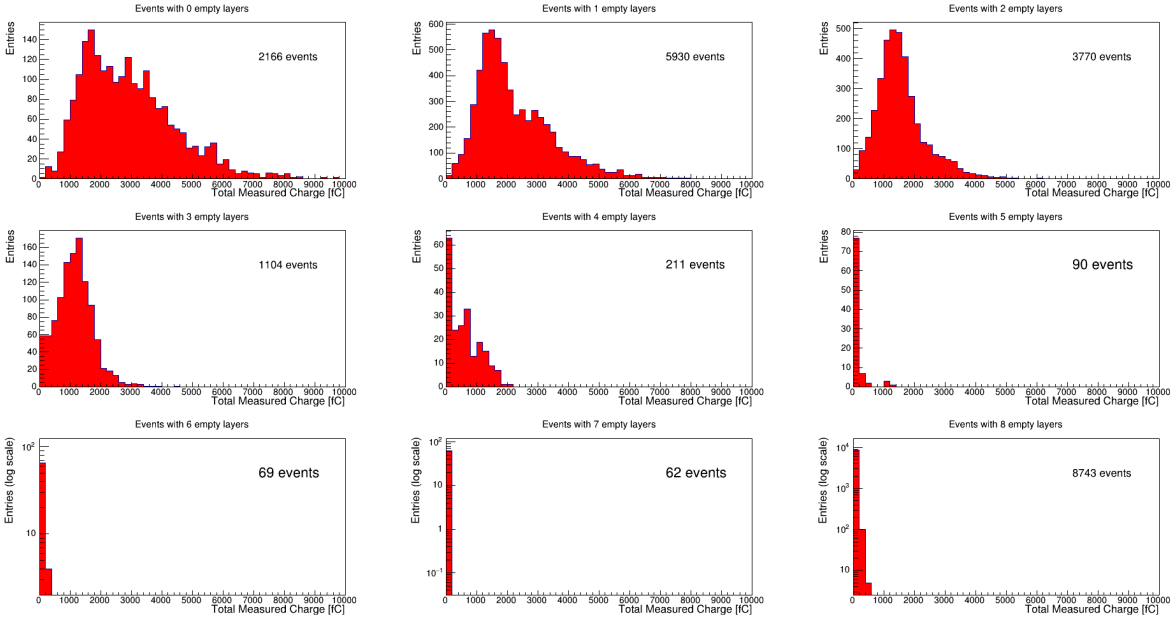

FIG. 34: The number of events with recorded charge deposits in a certain number of layers. Roughly 40% of events only deposit charge in one layer of the detector.

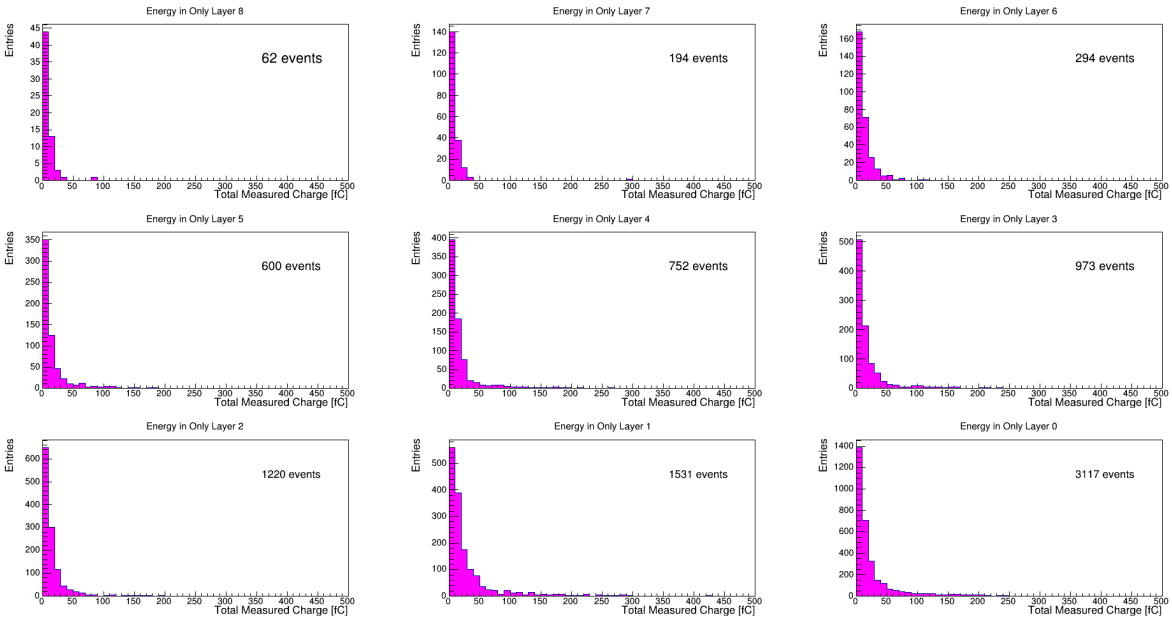

FIG. 35: For events that only deposit charge in one single layer of the detector, the layer of detected charge deposition is shown. Nearly 67% of these events deposit deep into the calorimeter (in Layer 2, 1, or 0) .

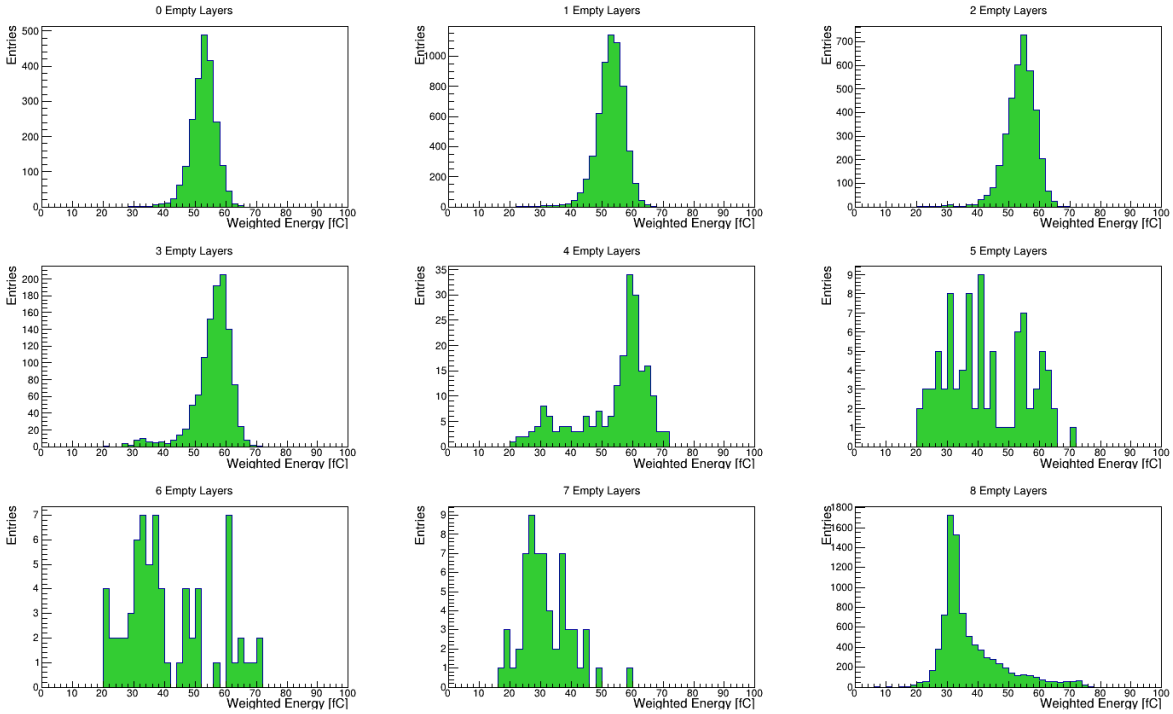

FIG. 36: Value of the statistic of Eqn. 1, separated by how many empty layers were in the event. Events with few empty layers had larger values of R, while events with many empty layers had low R values and were categorized as contamination when $R < 44$.

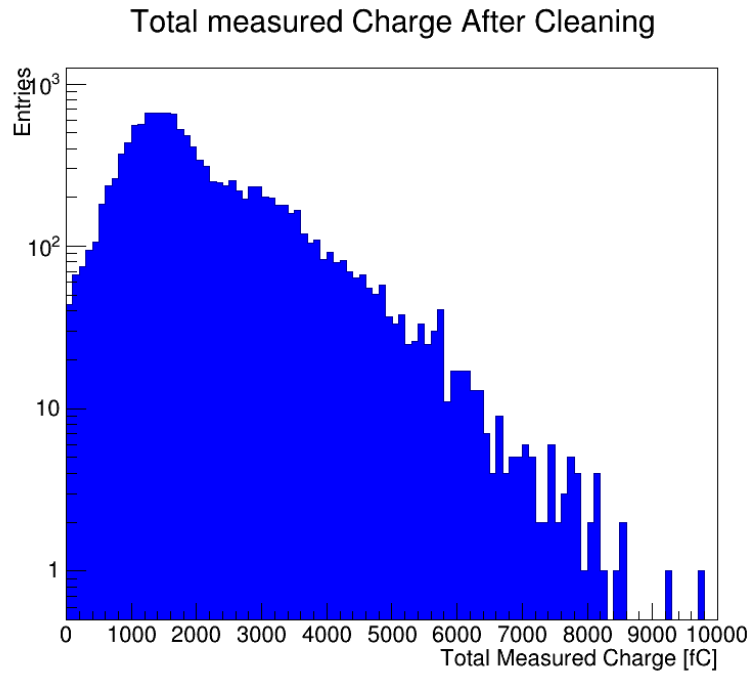

FIG. 37: Deposited charge data from the beam test where the silicon layer was placed first, after removing contamination.

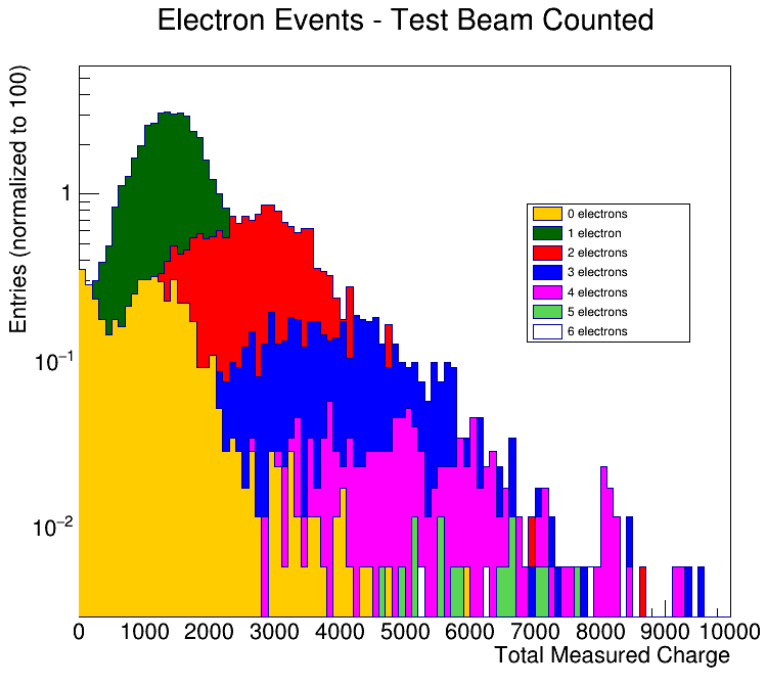

FIG. 38: Distributions of the number of counted electrons in silicon-first beam test Run 28.

B. Fitting for Parameters

A number of parameters used throughout the analysis stem from fitting the experimental beam test data. Figure 10 illustrates that one-electron events have a Gaussian-like distribution, so a Poisson-distributed series of Gaussian curves can be fit to the large collection of events from one- to five- simultaneous electrons. This involves the parameters $\langle n \rangle$ for the appropriate Poisson mean and a for a horizontal scale or conversion factor between the beam test units fC and simulation units MeV. It also requires inputs of E_0 (the mean energy of the Gaussian), n (the number of incident electrons), and σ_{MC} (the standard deviation of the Gaussian that results from the Monte Carlo simulation) (Figs. 10 and 17). It is this standard deviation that may be lacking in a simulation where unanticipated experimental effects are not considered (as mentioned in Sec. III), so an additional parameter σ is added to the fit to find the degree of variation between the Monte Carlo's standard deviation and that of the experimental data set. The fitting equation then is

$$\begin{aligned} D(E) &= \sum_{n=1}^{\infty} P(n, \langle n \rangle) \mathcal{E}(E, anE_0, a^2 n(\sigma_{MC}^2 + \sigma^2)) \\ P(n, \langle n \rangle) &= \frac{\langle n \rangle^n}{n!(e^{\langle n \rangle} - 1)} \\ \mathcal{E}(E, anE_0, a^2 n(\sigma_{MC}^2 + \sigma^2)) &= \frac{1}{\sqrt{2\pi n}\sqrt{\sigma_{MC}^2 + \sigma^2}} \exp\left[\frac{-(E - anE_0)^2}{2a^2 n(\sigma_{MC}^2 + \sigma^2)}\right] \\ \Rightarrow D(E) &= \frac{1}{a\sqrt{2\pi}\sqrt{\sigma_{MC}^2 + \sigma^2}(e^{\langle n \rangle} - 1)} \sum_{n=1}^{5} \frac{\langle n \rangle^n}{n!\sqrt{n}} \exp\left[\frac{-(E - anE_0)^2}{2a^2 n(\sigma_{MC}^2 + \sigma^2)}\right] , \end{aligned} \tag{2}$$

where the sum runs from $n = 1, \ldots, 5$ because events are only modeled with up to five incident electrons.

The resulting fits are shown for silion-first Run 43 in Fig. 39. The output parameters for this fit are shown in Table VIII B and used throughout this analysis.

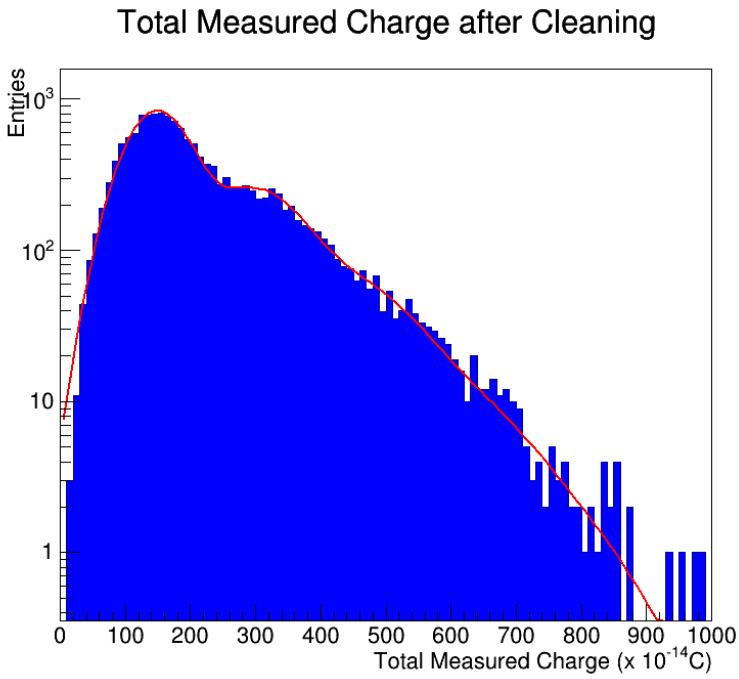

FIG. 39: Silicon-first beam test Run 43 fit by Eqn. 2 with inputs from the simulated single-electron distribution. The fitting parameters represent the Poisson mean $\langle n \rangle$, horizontal scaling a or the conversion factor from units of fC to MeV, and extra fluctuations observed in the experimental run but not taken into account within the simulation.

TABLE II: Fit parameters from fitting Eqn. 2 to beam test data runs.

Beam Test Run	$\langle n \rangle$	a	σ
43	0.906 ± 0.017	28.85 ± 0.17	$(7.04 \pm 4.02) \times 10^{-5}$
28	0.839 ± 0.015	30.3 ± 0.16	$(-1.46 \pm 0.9) \times 10^{-4}$
Si-first average	0.8725 ± 0.011	29.575 ± 0.12	0
24	0.773 ± 0.02	29.39 ± 0.2	102.3 ± 5.7

[1] T. Behnke, J. Brau *et al.*, "The Interntional Linear Collider Technical Design Report - Volume 4: Detectors," arXiv: 1306.6329v1[physics.ins-det]

[2] J. Brau, M. Breidenbach *et al.*, "KPiX - A 1,024 Channel Readout ASIC for the ILC," SLAC-PUB-15285 (2013), 2012 IEEE Nuclear Science SYmposium, http://slac.stanford.edu/pubs/slacpubs/15250/slac-pub-15285.pdf

[3] M. Breidenbach *et al.*, "Prototype silicon — tungsten Ecal with Integrated Electronics: First Look with beam test," 2013 Linear Collider Workshop (LCWS), Tokyo, https://agenda.linearcollider.org/event/6000/contributions/27576/